ELSEVIER

Applied Ocean Research 23 (2001) 29–40

Applied Ocean Research

www.elsevier.com/locate/apor

On the non-linear forces acting on a floating spar platform in ocean waves

Q.W. Ma*, M.H. Patel

Department of Mechanical Engineering, University College London, Torrington Place, London WC1E 7JE, UK

Received 14 January 2000; revised 16 November 2000

Abstract

The exploitation of hydrocarbon reservoirs under the seabed in very deep water requires the use of innovative floating platform configurations. The hydrodynamic interaction of such platforms with ocean waves and the understanding and quantification of the non-linear components of these interactions have been a subject of continuing research. This paper examines these non-linear interaction components for a specific very deep draft spar platform type that is increasingly being used in the oceans. It investigates a formulation for two non-linear force components — called the axial divergence force and the centrifugal force. The latter is invariably neglected in conventional analyses but is shown in this paper to actually be of significant importance. Non-linear equations for wave loading and motion are developed and solved, and the results are used to demonstrate the significance of the above terms. A limited comparison with experimental data is also presented.

Keywords: Spar platform; Non-linear forces; Numerical simulation; Non-linear equation of motion

1. Introduction

As the offshore industry depletes hydrocarbon reservoirs below the sea bed in small to moderate water depths (up to 500 m), it is increasingly required to develop such deposits in considerably deeper water. The high water depth makes the use of sea bed mounted platforms uneconomic leaving a variety of floating platform types as the only viable options for oil and gas production operations. One such option is the spar platform which is basically a very large floating vertical cylindrical structure of around 200 m draft and 40 m or so in diameter. Such hull configurations have been shown to have several advantages over other options such as tension leg platforms and ship shape hulls. Some of these advantages include structural simplicity, low motions in moderate and extreme ocean waves because of their relatively long natural periods, good protection of riser connections to the sea bed, low cost and so on — Vardeman et al. [1] give an overview of the merits and drawbacks of Spar platforms.

Spar platforms are not new — smaller versions have been built, including the US Navy spar for gathering oceanographic data [2], the recently decommissioned Brent spar for oil storage [3], the Agip spar for flaring gas and a loading spar on the Draugen field [4]. Very recently, the first production spar in the world was installed in 1997, at Viosca Knoll 826, Gulf of Mexico, the first use of a very large spar in very deep water [4]. Fig. 1 presents a sketch of the structure and its mooring system.

In recent years the realisation that large spar platforms did offer low cost production options in very deep water has prompted several experimental studies and numerical simulations to obtain a better understanding of their response to ocean waves. Two such experimental studies are reported by Weggel et al. [5] and by Carpenter et al. [6]. Research using numerical simulations has utilised the two traditional frequency domain and time domain approaches. One such is presented by Weggel et al. [5] using the frequency domain technique — it directly gives the statistical parameters of the spar response at relatively low computational cost. However, it may be subject to large errors due to the linearisation of some non-linear terms, such as the viscous term, in the equations of motion. There is evidence that this linearisation probably overestimates viscous effects [7]. Most researchers prefer, therefore, to simulate spar motion in the time domain and this is the approach adopted in this paper.

Simulation of the motion of a spar buoy requires the definition of the equations of motion and the evaluation of all forces acting on it due to wind, current, ocean waves and mooring lines. The conventional approach in offshore engineering is to use the linear form of the equations to describe the motions of rigid bodies. For large motions the non-linear equations of motion [8] should be used but it is

* Corresponding author. Tel.: +44-20-7679-3866.
E-mail address: q.ma@meng.ucl.ac.uk (Q.W. Ma).

0141-1187/01/$ - see front matter
PII: S0141-1187(00)00025-0

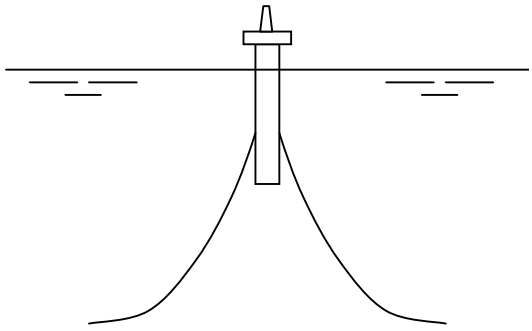

Fig. 1. A spar platform.

only practicable if the exciting forces can be calculated without involving wave diffraction analysis.

A key element of the analysis of a spar buoy is to evaluate the forces and moments on it due to ocean waves and currents. One possibility to obtain these is to perform a numerical analysis of the fully non-linear interaction between the spar and its surrounding fluid. Although it is not impossible, this task requires very powerful computer resources and is, therefore, not feasible in practice. An alternative approach is to carry out a diffraction analysis based on second order potential theory (see, for example, Ran et al. [7]). The computational cost of this approach is still quite high. Also, this method usually generates results in the frequency domain and thereafter a transformation is needed to obtain forces in the time domain.

Another approach, often used in offshore engineering for wave force evaluation, is based on slender body theory that requires much less computational effort and can be directly implemented in time domain analysis. In this approach, the body is assumed 'thin' and the force (and/or moment) is obtained by the sum of the force on each short segment of the slender body. The force on each segment is decomposed into two parts — an inviscid force and a viscous drag force. One typical slender body wave force formulation is the well-known Morison equation, in which the first part is proportional to the relative acceleration and the second part to the product of the relative velocity. In addition, Rainey [9,10] has derived an alternative formula for the inviscid force on a slender body. His approach modifies the Morison equation by including axial divergence and centrifugal force terms acting on the spar body cross-section and by introducing additional point forces at the two ends of the body. All of these forces are non-linear and do not appear in the normal Morison equation formulation. Several computational studies have been reported in the research literature using the slender body approach-all of them using different methods to calculate the inviscid force. Chitrapu et al. [8] approximated the inviscid force by the sum of a 'Froude–Krylov' force and inertia force. The latter is evaluated in the same way in the Morison equation but the former is estimated by the integration of the fluid pressure over the spar hull in undisturbed flow. Mekha et al. [11] considered the convective acceleration of the fluid and the axial divergence term given by Rainey [9,10], but showed in their case that the axial divergence term is not very important. One of the main differences between the work is in the employment of non-linear inviscid force terms.

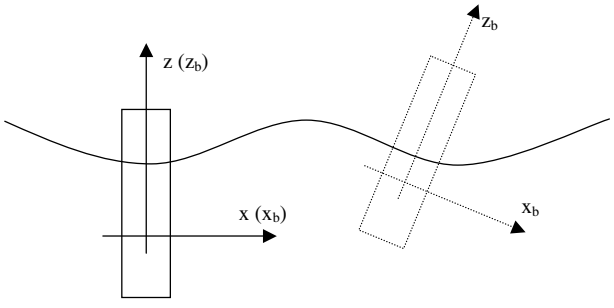

Fig. 2. The reference co-ordinate system for a spar platform.

All of the results published by the above authors have demonstrated that the slowly varying surge and pitch motion may be much greater than the responses at the incident wave frequency. This implies that non-linear effects play a very important role in spar buoy performance and that the non-linear force and moment need to be considered with great care. The main purpose of this paper is to consider all the terms involved in a full slender body formulation and to investigate the relative importance of the non-linear terms in this formulation. Particular attention is paid to the axial divergence, the centrifugal and point forces that have either been totally excluded or have been dealt with to a limited extent in the past. The methodology employed uses the fully non-linear equations of motion with the mooring lines replaced by springs.

One question that does arise in considering slender body theory, is its accuracy when applied to spar platforms. According to the derivation of Manners and Rainey [12] and the discussion by Rainey [9], the errors in using slender body theory are of the order of $(D/\lambda)^3$, where λ is the wavelength and D is the diameter of the cylinder. Thus as long as the ratio (D/λ) is small enough, the theory can be sufficiently accurate. Kim and Chen [13] compared results from slender body theory with those from the diffraction analysis for the second-order force acting on a fixed articulated platform, and showed that the slender-body approximation could give very similar results to those of diffraction theory when the length scale of the structure is small (say less than 20%) relative to the wave length. The work of this paper also follows this criterion for the validity of slender body theory.

2. Equations of motion and forces

In order to describe the motion of a spar platform, two co-ordinate systems are used, as illustrated in Fig. 2. $Oxyz$ is a space-fixed system with its z-axis being upward and its origin at the centre of gravity of the spar when it is at rest. $O_b x_b y_b z_b$ is a body-fixed system with its z_b-axis along the centreline and its origin always at the centre of gravity,

and so is moving with the body. When the spar is at the rest, the two systems coincide with each other.

The spar platform is considered as a rigid body. Its state and attitude can be described by the translational displacement ($\boldsymbol{X}$) and velocity ($\boldsymbol{U}_0$) of its centre of gravity, Euler angles ($\boldsymbol{\theta} = \{\alpha, \beta, \gamma\}$) and angular velocity ($\boldsymbol{\Omega}$). The general non-linear equations of motion for a rigid body are well known and can be written as:

$$[M]\frac{\mathrm{d}\boldsymbol{U}_0}{\mathrm{d}t} = \boldsymbol{F} \tag{1}$$

$$[I]\frac{\mathrm{d}\boldsymbol{\Omega}}{\mathrm{d}t} + \boldsymbol{\Omega}\times[I]\boldsymbol{\Omega} = \boldsymbol{N} \tag{2}$$

$$\frac{\mathrm{dX}}{\mathrm{d}t} = \boldsymbol{U}_0 \tag{3}$$

$$[B]\frac{\mathrm{d}\boldsymbol{\theta}}{\mathrm{d}t} = \boldsymbol{\Omega} \tag{4}$$

where $\boldsymbol{F}$ is the total external force, $\boldsymbol{N}$ the moment of the force about the centre of gravity, $[M]$ and $[I]$ are the mass and inertia matrix, respectively and $[B]$ is a matrix formed by Euler angles (α, β, γ), defined by Ma [14], Eq. (3.3.18).

$$[B] = \begin{bmatrix} \cos\beta\cos\gamma & \sin\gamma & 0 \\ -\cos\beta\sin\gamma & \cos\gamma & 0 \\ \sin\beta & 0 & 1 \end{bmatrix} \tag{5}$$

For convenience, the translation motion equations (1) and (3) have been written in terms of components of vectors in the $Oxyz$ system while the rotational equations (2) and (4) have been written in terms of components in the $O_b x_b y_b z_b$ system. Therefore, all non-diagonal entries in matrices $[M]$ and $[I]$ are actually zero, and $I_{xx} = I_{yy}$ if the distribution of the mass is axisymmetric. Furthermore, if the spar has no initial angular velocity, it can be shown that $\boldsymbol{\Omega}_{z_b} = 0$ and so $\boldsymbol{\Omega}\times[I]\boldsymbol{\Omega} = 0$, under the slender-body assumption. That means the spar actually has only 5 degrees of freedom.

The forces and moments appearing on the right-hand side of Eqs. (1) and (2) are evaluated based on slender body theory. The forces due to inviscid flow given by Rainey [10] are used, and the drag force in the Morison equation is employed to account for viscous effects. According to Rainey [10], the force due to inviscid flow may have four parts but one of them appears to be zero for a circular cylinder. This formula is applied here for the circular cylindrical spar hull and is written as follows:

2.1. Force per unit immersed length ($d\boldsymbol{F}_1$)

$$d\boldsymbol{F}_1 = \rho S\{\boldsymbol{a} - \boldsymbol{g}\}_n + [M_a]\{\boldsymbol{a} + (\boldsymbol{l}\cdot[V]\boldsymbol{l})\boldsymbol{w}\} - [M_a]\dot{\boldsymbol{U}} - 2[M_a]\tilde{\boldsymbol{\Omega}}\boldsymbol{w}_A \tag{6}$$

where, $\boldsymbol{a} = (\partial\boldsymbol{v})/(\partial t) + [V]\boldsymbol{v}$ with $\boldsymbol{v}$ and $\{V\}$ being the velocity and velocity gradient matrices of the incident wave, respectively. $\boldsymbol{U}$ is the velocity of the body at the corresponding point, i.e. $\boldsymbol{U} = \boldsymbol{U}_0 + \boldsymbol{\Omega}\times\boldsymbol{r}$ ($\boldsymbol{r}$ is a vector from the centre of gravity to the relevant point). $[M_a]$ is the added mass matrix and satisfies $[M_a]\boldsymbol{r} = 0$. $\tilde{\Omega}$ is a matrix composed of the components of angular velocity and defined by $\tilde{\boldsymbol{\Omega}}\boldsymbol{x} = \boldsymbol{\Omega}\times\boldsymbol{x}$ for any axial vector $\boldsymbol{x}$. $\{\ \}_n$ denotes the transverse components normal to the axis of the spar. $\boldsymbol{g}$ is the gravitational acceleration, pointing downwards, i.e. $\boldsymbol{g} = -g\boldsymbol{e}_z$, $\boldsymbol{w} = \boldsymbol{v} - \boldsymbol{U}$ is the relative velocity with $\boldsymbol{w}_A$ being its axial component, S is the cross-section area of spar hull and $\boldsymbol{l}$ is an upward unit vector along the spar centreline.

The terms in the first pair of braces in Eq. (6) are the Froude–Krylov force plus the transverse static buoyancy. They are the force components acting on the spar segments from both the wave-induced dynamic and hydrostatic pressure in the undisturbed surrounding fluid and include the hydrostatic forces due to non-zero angles of the spar from the vertical. The forces due to the disturbance of the surrounding fluid by the spar are considered in subsequent terms — one of these corresponding to the normal diffraction force represented by the first term in the second pair of braces. The second term in these braces

$$[M_a]\{(\boldsymbol{l}\cdot[V]\boldsymbol{l})\boldsymbol{w}\} = \left(l\cdot\frac{\partial\boldsymbol{v}}{\partial l}\right)[M_a]\boldsymbol{w}$$

is called the axial divergence force. According to Manners and Rainey [12], this term can be interpreted as the force caused by a decrease of the added mass per unit length due to the divergence of the axial incident flow. If the incident flow in the direction of the spar centerline is a constant along the spar, this term is zero. Otherwise, the force arises from the velocities of the incident flow and the spar motion. The term, $[M_a]\dot{\boldsymbol{U}}$, in Eq. (6) corresponds to the normal radiation force due to the acceleration of the spar. The last term in that equation is proportional to the cross product of angular velocity and the relative velocity in the axial direction. This is similar in some sense to the well-known Coriolis force acting on a particle moving in a non inertial co-ordinate system. In some simple cases such as a thin body moving in a circle, this term is also able to be interpreted as 'negative centrifugal force' (Rainey, [9,10]). In this paper, the term is called centrifugal force following Rainey [10].

2.2. Point force at an immersed end

This is given by:

$$\boldsymbol{F}_2 = pS\boldsymbol{l} - (\tfrac{1}{2}\boldsymbol{w}\cdot[M_a]w)\boldsymbol{l} + (\boldsymbol{l}\cdot w)[M_a]w \tag{7}$$

where $p = p_h + p_s$ is the sum of hydrodynamic and static water pressures — the second of which provides the axial buoyancy and hydrostatic restoring force together with the term of $\{-\boldsymbol{g}\}_n$ in Eq. (6). The velocity squared term in the expression for pressure together with the second and third

term in Eq. (7) provides a force that is of second order of wave amplitude.

2.3. Point force at spar buoy–water surface intersection

This force is given by:

$$\boldsymbol{F}_3 = \tfrac{1}{2}\tan\alpha[(\boldsymbol{t}\cdot\boldsymbol{w})[M_a]\boldsymbol{w} - (\boldsymbol{t}\cdot(\boldsymbol{l}\times[M_a]\boldsymbol{w}))(\boldsymbol{l}\times\boldsymbol{w})] \tag{8}$$

where α is the acute angle between the centreline of the spar and the free-surface normal vector of the undisturbed wave; and $\boldsymbol{t}$ is a unit vector in their joint plane, normal to the spar axis and pointing out of the fluid. If the spar has no initial inclination, $\tan\alpha$ is determined by the motion of the spar and the wave, and such a point load is of third order with respect to the wave amplitude.

In addition to the above inviscid force, the drag force per unit length is expressed by:

$$\mathrm{d}\boldsymbol{F}_{\mathrm{drg}} = \rho R_0 C_{\mathrm{D}}|\boldsymbol{w}_n|\boldsymbol{w}_n \tag{9}$$

where C_{D} is the drag coefficient and $\boldsymbol{w}_n$ is the component of $\boldsymbol{w}$ normal to the spar axis.

From Eqs. (6) and (9), the total force and moment acting on the spar can be written as:

$$\begin{aligned}\boldsymbol{F} &= \int_L \mathrm{d}\boldsymbol{F}_1 + \int_L \mathrm{d}\boldsymbol{F}_{\mathrm{drg}} + \boldsymbol{F}_2 + \boldsymbol{F}_3 \\ &= \boldsymbol{F}_{\mathrm{m}} + \boldsymbol{F}_{\mathrm{a}} + \boldsymbol{F}_{\mathrm{div}} + \boldsymbol{F}_{2\mathrm{v}} + \boldsymbol{F}_{\mathrm{drg}} + \boldsymbol{F}_{\mathrm{bp}} + \boldsymbol{F}_{\mathrm{sp}} + \boldsymbol{F}_{\mathrm{g}} + \boldsymbol{F}_{\mathrm{mr}}\end{aligned} \tag{10}$$

$$\begin{aligned}\boldsymbol{N} &= \int_L \boldsymbol{r}\times\mathrm{d}\boldsymbol{F}_1 + \int_L \boldsymbol{r}\,\mathrm{d}\boldsymbol{F}_{\mathrm{drg}} + \boldsymbol{r}_{\mathrm{e}}\,\boldsymbol{F}_2 + \boldsymbol{r}_{\mathrm{f}}\,\boldsymbol{F}_3 + \boldsymbol{r}_{\mathrm{mr}}\,\boldsymbol{F}_{\mathrm{mr}} \\ &= \boldsymbol{N}_{\mathrm{m}} + \boldsymbol{N}_{\mathrm{a}} + \boldsymbol{N}_{\mathrm{div}} + \boldsymbol{N}_{2\mathrm{v}} + \boldsymbol{N}_{\mathrm{drg}} + \boldsymbol{N}_{\mathrm{bp}} + \boldsymbol{N}_{\mathrm{sp}} + \boldsymbol{N}_{\mathrm{g}} \\ &\quad + \boldsymbol{N}_{\mathrm{mr}}\end{aligned} \tag{11}$$

where L is the wetted length of the spar; $\boldsymbol{F}_{\mathrm{mr}}$ (or $\boldsymbol{N}_{\mathrm{mr}}$) is the force (or moment) due to the mooring line; $\boldsymbol{r}_{\mathrm{e}}$, $\boldsymbol{r}_{\mathrm{f}}$ and $\boldsymbol{r}_{\mathrm{mr}}$ are the position vectors of the immersed end, the intersection point and the fairleads of mooring line to the centre of gravity, respectively. For ease of explanation in the following, the force components have been rearranged to give components with different subscripts. Subscript a represents the force and moment due to fluid acceleration; div due to an axial divergence term; 2v due to a centrifugal term; drg due to the drag term; bp due to the point load at the immersed end excluding the static pressure; sp due to the force at the free-surface intersection and g represents the force due to the static pressure including $\mathrm{p_s}$ in Eq. (7) and $\rho S\{-\boldsymbol{g}\}_n$ in Eq. (6). The force $\boldsymbol{F}_{\mathrm{m}}$ and moment $\boldsymbol{N}_{\mathrm{m}}$ depend on the acceleration of the body. These terms will be moved to the left-hand side of Eqs. (1) and (2) to make them more suitable for time-domain integration. The details of this reformulation can be found in Pauling and Webster [15].

The above integration to obtain the forces and moments is performed on the instantaneous wetted centreline of the spar. This means that the wave parameters are evaluated at instantaneous positions with the length L changing with time due to the relative motion between the spar and the free surface. The resultant terms are given in Eqs. (10) and (11). The following components of the non-linear force can be readily identified within these equations: (a) the acceleration of the fluid; (b) the axial divergence term; (c) the centrifugal force; (d) the drag force; and (e) the two point forces at the immersed end and at the intersection of the free surface. The non-linearity of all the terms except for (a) results from the products of the wave and motion parameters as well as the influence of the change of position and wetted length of the spar. For component (a), the non-linearity also arises from the temporal acceleration in addition to the convective acceleration, the latter of which is from the product of wave parameters. The non-linearity from the former is caused solely by the change of position and wetted length of the spar. Terms (a) and (d) have been considered by all authors who use slender body theory. The axial divergence term was taken into account by Mekha et al. [11] but it was suggested to be very small in their cases. Part of the influence of $\boldsymbol{F}_{\mathrm{bp}}$ and $\boldsymbol{N}_{\mathrm{bp}}$ could have been taken into account by Chitrapu et al. [8] if the integration on the incident wave pressure had been performed over the whole spar wetted surface including the immersed end (although it is not clear if this was actually done or not). The effect of centrifugal force, which is clearly of the same order in wave amplitude as the other non-linear terms, has not been considered to date. Although the point force at the free surface is not taken into account in the literature either, it may not play an important role because this term is of higher order than the others. The work presented below investigates the relative importance of the centrifugal force, the axial divergence force and the point force at the immersed end. It will be shown that the effect of these forces is significant in practical circumstances.

It should be noted that the above formula may not give mean drift force correctly because the drift force from the formula is zero in some special cases where it should not be. Mekha et al. [11] included the drift force using empirical expressions and investigated their effects on spar motions. They showed that the inclusion of the drift forces can make the mean offset closer to the experimental results but it has little influence on the oscillatory motion. This paper is concerned with the effects of the non-linearities on the spar buoy oscillatory motion, and consequently does not consider the mean drift force.

3. Numerical procedure

The system of equations described above is highly non-linear, not only because some products of motion parameters in Eq. (4) are included but also because the evaluation of all the forces and moments are dependent on the position, velocity and acceleration of the spar, which are

not known before solving the equations. In order to solve this system of equations, the following numerical procedure is employed:

(1) Start from an initial state in which the displacement and velocity of the spar are zero (or with any other known values), and the parameters of the wave are given.
(2) Find the length of the wetted spar hull.
(3) Evaluate the force and moment vectors by numerical integration.
(4) Solve the motion equations to give the new position and velocity of spar.
(5) Go to step (2) and repeat.

3.1. Instantaneous length of spar

In order to determine the instantaneous length of the spar, one needs to find the common point of the spar centreline and the free surface. This is actually equivalent to finding the common point between a three-dimensional curved surface and a straight line in space. Since the surface changes with time, and the attitude of the spar is determined during the process of the solution, this point has to be found in each time step. Although this is quite straightforward, a suitable function needs to be constructed for implementing the numerical solution. To do so, the free surface and the centreline of the spar are expressed by the following two equations, respectively:

$$z = \zeta(x, y, t) \quad \text{for wave}$$

$$\begin{cases} z = A_1(t)x + B_1(t)y + C_1(t) \\ z = A_2(t)x + B_2(t)y + C_2(t) \end{cases} \quad \text{for the spar}$$

Then the co-ordinates of the common point (x_s,y_s,z_s) should satisfy the equation:

$$\{\zeta(x_s, y_s, t) - [A_1(t)x_s + B_1(t)y_s + C_1(t)]\}^2 + \{\zeta(x_s, y_s, t) - [A_2(t)x_s + B_2(t)y_s + C_2(t)]\}^2 = 0$$

This is equivalent to minimising the following function:

$$G(x_s, y_s, t) = \{\zeta(x_s, y_s, t) - [A_1(t)x_s + B_1(t)y_s + C_1(t)]\}^2 + \{\zeta(x_s, y_s, t) - [A_2(t)x_s + B_2(t)y_s + C_2(t)]\}^2$$

The simplex method is used to minimise $G(x_s,y_s,t)$ with the tolerable error being taken as 0.0001. This method requires evaluations of functions only without a need for derivatives of functions that are computationally expensive to find. In addition, this method is also fast if a good initial estimate of the minimum can be specified for the problem. In this case, the co-ordinates of the intersection point between the spar centreline and the mean free surface can be taken as the initial estimate.

3.2. Evaluating the force and moment

After the instantaneous wetted length of the spar is found, the forces and moments can be evaluated using a numerical integration method. In this work, an adaptive recursive Simpson's rule is employed. As is well known, a feature of the method is that the number of divisions along the spar will be automatically doubled if the error tolerance is exceeded. This feature can reduce the computational cost in the sense that no more than the necessary computation is needed to achieve the desired accuracy. Its disadvantage is that the segments are halved uniformly according to a global error estimate, and so when the integrand changes rapidly in some areas and distributes quite uniformly in others, the segments in the latter part of the domain may become too small. In this case, since the wave parameters decay exponentially with water depth and the spar hull is very long, the property of the integrand must be very different in the area near the immersed end and in the area near the free surface. If the adaptive recursive Simpson's rule is simply used over the whole spar hull, it can be expected that the segments in the lower part of the spar may become unnecessarily small so that the computational cost is higher. To avoid this, the spar is first divided into a number of parts, e.g. five parts along its centreline, and then the adaptive recursive Simpson's rule is applied to each of the parts in turn. The relative error tolerance (ϵ_1) needed in this rule to control the process is chosen so that further reduction of ϵ_1 leads to a negligible difference.

3.3. Solving the equations of motion

The equations of motion are a system of first order, nonlinear ordinary differential equations with $\boldsymbol{X}$, $\boldsymbol{\theta}$, $\boldsymbol{U}_0$ and $\boldsymbol{\Omega}$ being the unknown variables. Some researchers [8] have used a fourth order Runge–Kutta method with a fixed step to solve the system and some have used the Newmark-β scheme. In this paper, the fifth order Runge–Kutta method with an adaptive stepsize control is used. The details of this method may be found in Shampine [16]. In this method, each time step is iteratively determined to achieve a desired accuracy. The relationship between the time step and estimated error is given by:

$$h_0 = \mu h_1 \left| \frac{\Delta_0}{\Delta_1} \right|^{0.2} \tag{12}$$

where μ is a coefficient chosen artificially — it is taken as 0.8 in this paper. Δ_1 is an error produced when the time step is taken as h_1. The value of Δ_1 is estimated based on the difference between the solution of the fifth-order Runge–Kutta method and the embedded fourth-order formula. In this specific case, there are several variables to be solved and Δ_1 is determined using the maximum error of the displacement components at a point away from the centre of gravity. The displacement at this point is

Table 1
Principal particulars of a spar platform

Diameter ($2R_0$)	40.5 m
Initial draft (L_0)	198.2 m
Mass (with entrapped water)	$2.6 \times 10^{+8}$ kg
Radius of gyration (pitch and roll)	62.33 m
Centre of gravity from keel	92.4 m
Fairleads from keel	92.6 m
Drag coefficient	$C_D = 0.6$
Added mass coefficient	$m_a = \rho S^a$
Density of water	$\rho = 1025$ kg/m^3

[a] S is the area of cross-section.

calculated by the angular and translational displacement of this centre. Although the velocity of the spar is not explicitly included in determining Δ_1, it is implicitly related to Δ_1 because the displacement is obtained by integrating the velocity. Δ_0 is the desired accuracy that is specified as $\Delta_0 = \epsilon_2 \max(\bar{X}, 10^{-6})$, where ϵ_2 is the relative error tolerance and $\bar{X}$ is the maximum of the three displacement components of the above point at previous time step. ϵ_2 has been determined by numerical tests.

3.4. Programming

The above methodology is programmed using MATLAB. In the code, $\epsilon_1 = \epsilon_2$ is used, leaving the choice of only one parameter associated with accuracy control, although the two error tolerances are not necessarily relevant. This choice makes the investigation of convergence simpler. If the error is small enough, the results should not be different from those obtained by using two different error tolerance values.

4. Results and discussion

The numerical calculations in the following are based on a large spar, which is very similar to the structure installed at the Viosca Knoll 826 field and has the same parameters as those used by Weggel et al. [5]. Table 1 presents the principal particulars of this platform design. The spar is positioned by four catenary mooring lines — two of them being in the *xoz* plane and the others in the *yoz* plane. In the simulation, each of the mooring lines is considered as a non-linear spring with its stiffness taken as 191 kN/m up to an offset of 13.7 m and 398 kN/m at offsets larger than this. The natural period of the spar for a linear response is about 328 s for surge, 68 s for pitch and 27 s for heave without accounting for viscous effects. In the simulation, a cosine taper function is imposed on the force and moment in order to reduce the transient effects produced by the impulsive nature of loading. Unless mentioned otherwise, the taper period is 50 s. The waves are assumed to propagate along the *x*-axis. With this configuration, the spar moves only in the *xoz* plane — surging, pitching and heaving. The following discussions are based on the results of the special case, but the methodology described in previous sections can be applied to general cases with any degrees of freedom.

4.1. Convergence

The first case presented here for the response of the spar uses incident monochromatic wave with the wave height being $H = 6$ m and the period being $T = 14\,s$, with and without current. As mentioned previously, the accuracy of the results may be controlled by the error tolerance variable in the integration of the force and in the solution of the equations of motion. Two values of this tolerances have

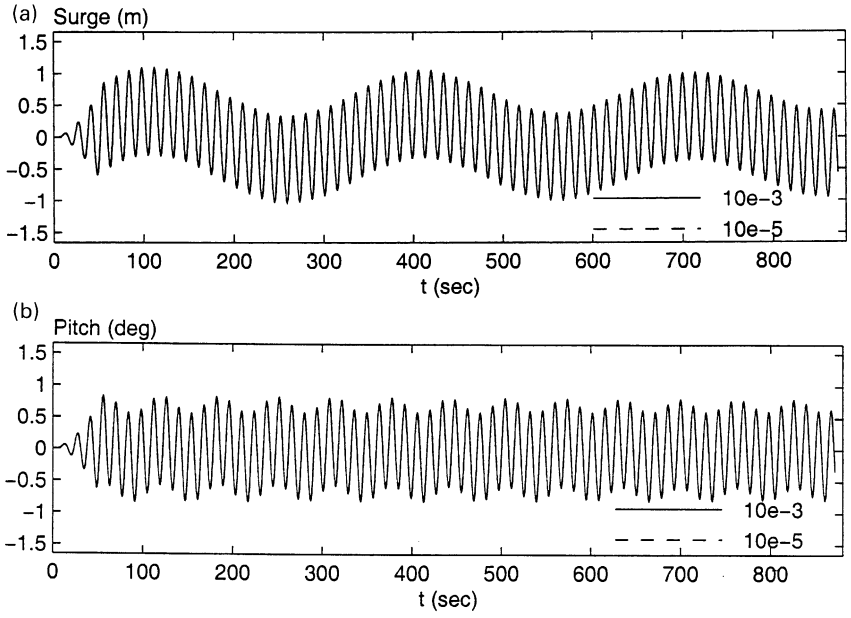

Fig. 3. The response of the spar subjected to waves without current. (a) Surge at the centre of gravity. (b) Pitch.

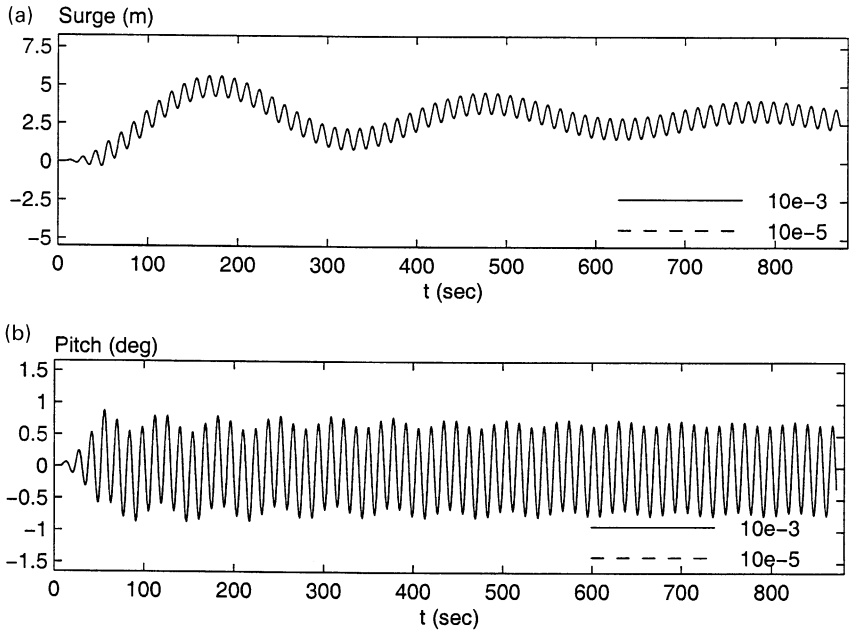

Fig. 4. The response of the spar subjected to wave with a constant current (0.5 m/s) (a) Surge at the centre of gravity. (b) Pitch.

been used: $\epsilon_1 = \epsilon_2 = 10^{-3}$ and $\epsilon_1 = \epsilon_2 = 10^{-5}$ for this case. The resultant surge and pitch motions are plotted in Fig. 3 for the case without current and Fig. 4 for the case with a constant current of 0.5 m/s with depth. It can be seen that the difference between the results corresponding to different error tolerance values is negligible, which implies that 10^{-3} may be small enough for these cases. It should be noted that a suitable error tolerance does depend on the wave, current and spar parameters, and therefore should be chosen accordingly. All the results presented in the following are obtained using $\epsilon_1 = \epsilon_2 = 10^{-5}$.

One interesting feature of the spar buoy responses is touched on here. It concerns the persistence of the long period oscillation of surge. The natural period in surge of the example spar buoy used here is about 328 s. Fig. 5 shows calculations carried out for a time scale of the order of 6000 s. The surge oscillation suggests very strongly that the long period oscillation seen here may be due to transient effects. This result reinforces the fact that damping in surge for spar buoys is so small that transient effects take a very long time to die away. Due to this effect, any analysis aimed at determining steady state parameters (such as motion spectrum) should be based on long periods of simulated or experimental results. This long transient phenomenon is not clearly identified in previous work on the spar buoys.

4.2. Comparison with experimental results

The published experimental results by Weggel et al. [5] are used here to check numerical results obtained in this work. Fig. 6 represents the pitch responses for two cases. The taper period here is about 200 s in order to simulate the start period in the experimental results. One case in this figure is the same as the above. Another case is for the spar subjected to bichromatic waves with periods and amplitudes being (16 s, 17.5 s) and (6 m, 6 m), respectively. Generally speaking, the numerical results have the same trends as experimental ones and the agreement is fairly

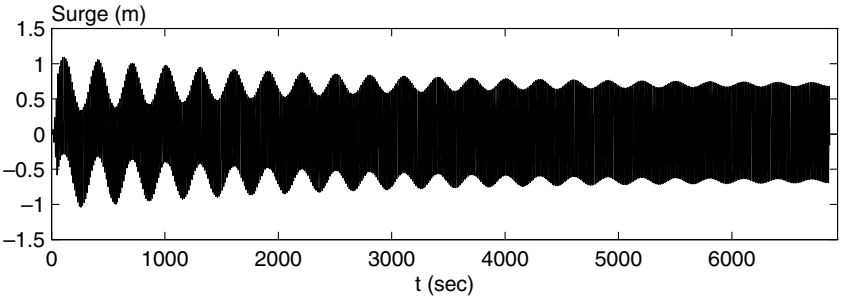

Fig. 5. The surge response over a longer time scale (all the parameters are the same as those in Fig. 3).

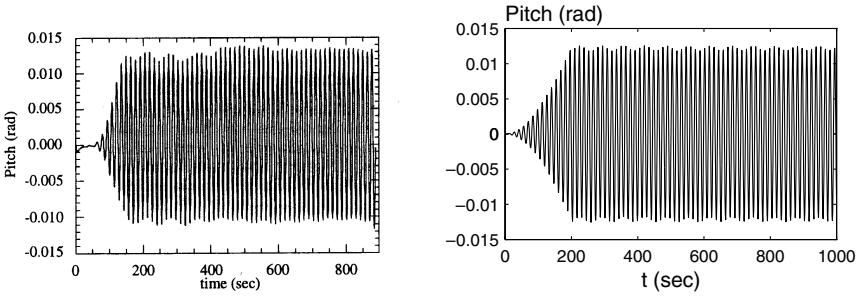

(a) Experimental results for monochromatic wave (b) Numerical results for monochromatic wave

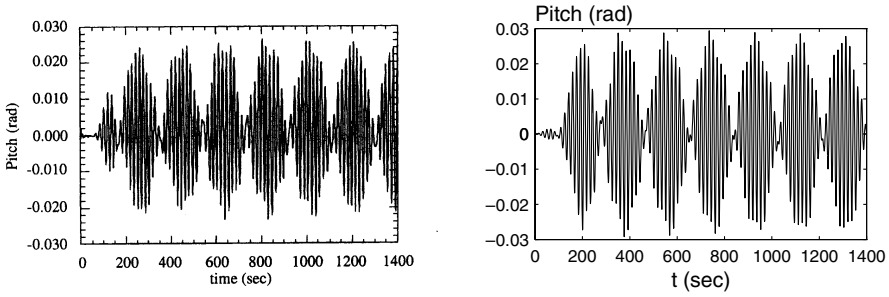

(b) Experimental results for bichromatic wave (c) Numerical results for bichromatic wave

Fig. 6. Comparison with experimental results for pitch of spar subjected to the mono- and bichromatic waves. (The experimental results are duplicated from Weggel et al. [5]).

good, although slight differences do exist. There is also similar good agreement for surge motion, and the figure is not given here for brevity. The small differences between the numerical solution and experiments may be due to the effects of mean drift force, the mooring line drag force (through coupling between the spar and mooring lines) and other factors not considered here.

4.3. Investigation of non-linear forces

As mentioned earlier, the centrifugal force has not been considered adequately yet in the research literature and the axial divergent force is either ignored or shown to be small. In this section, these two components and the point forces at the immersed end of the spar are compared with the non-linear component from the acceleration of the fluid. The last is obtained by subtracting the linear part, which is the integration of the temporal acceleration of fluid at the mean position (fixed position and length) of the spar, from the total value by integrating the whole acceleration term on the instantaneous position of the spar.

Fig. 7 presents the time histories of the non-linear surge force components when the spar is excited by a monochromatic wave with $H = 9$ m and $T = 16$ s. Here the fa2 term represents the non-linear force from acceleration, the fdiv term is the axial divergent force, f2v represents the centrifugal force and fbp is the point force at the immersed end of the spar. It can be seen that in this case each of the amplitudes of fdiv and f2v are about 50% of that of fa2 while fbp is about a third of fa2. This is one example that demonstrates that fdiv, fdiv and fbp should be taken into account when compared to fa2. The relative values of these components to fa2 clearly depend on the wave parameters for any given spar. In order to investigate the behaviour of these non-linear forces in a more general case, the calculations and comparisons have been carried out below for different wave period and amplitudes.

In order to usefully compare the non-linear forces for various cases, the oscillation heights of the forces are used — measured from minimum to maximum during the steady part of their time histories. The incident wave in these calculations is similar to that used above but the wave height and period are varied. In Fig. 8, the various non-linear components of the surge force corresponding to different wave periods are plotted with the oscillation heights of the forces non-dimensionalised by $(1/2)\rho g R_0 H^2$. The wave height used to obtain the results is $H = 9$ m. It can be seen from Fig. 8 that in the range of shorter periods, fa2 dominates over the other terms; and fdiv is smaller than fa2 but evidently larger than the other two. With increase in wave period, however, fa2 and fdiv decrease while the other terms tend to increase. When the period is large, f2v can become as large as fa2 while fdiv can become much smaller than others. It can clearly be seen that the importance of each non-linear

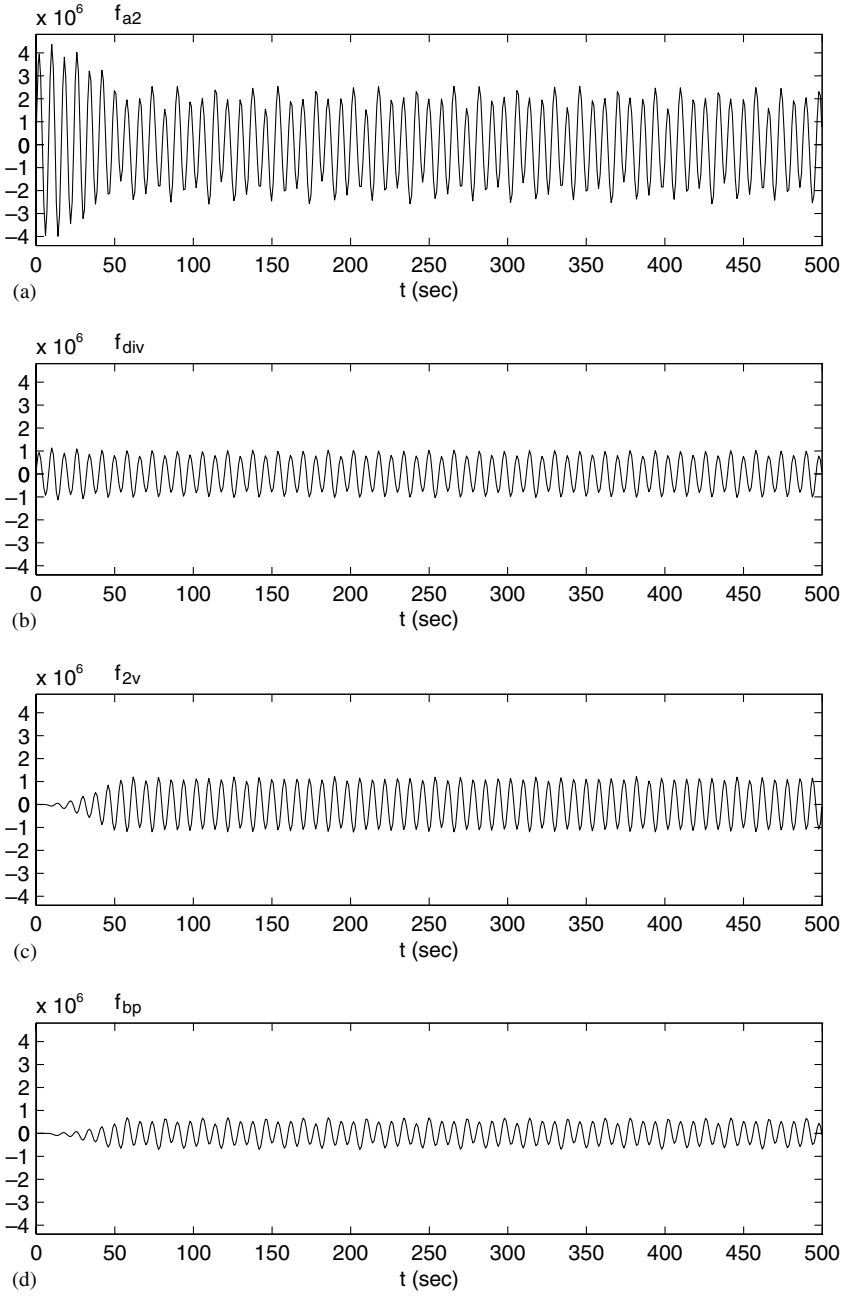

Fig. 7. The time history of various non-linear forces ($H = 9$ m and $T = 16$ s).

component largely depends on the wave period, and that the centrifugal force, the point force and the axial divergent force may not always be negligible compared to fa2.

The relative magnitudes of the force term are examined as a function of wave height next. Figs. 9 and 10 present the variation of these forces with wave heights for periods of 14 and 16 s, respectively. As before, the forces are non-dimensionalised by division with $(1/2)\rho g R_0 H^2$. The axial divergent force in Fig. 9 is larger than the centrifugal force. In Fig. 10, however, the former is smaller than the latter, and both are closer to fa2 than in Fig. 9. This relationship continues to hold when the wave height increases.

Similar comparisons have also been made for the moments corresponding to the above force components. These comparisons show that the non-linear moment due to the acceleration of the fluid largely dominates over the other components. The reason may be due to the fact that the non-linear part of fa2 is mainly concentrated on the area near the water line, while the distribution of the other forces such as fdiv and f2v are relatively flat along the spar. Therefore, even though fdiv and f2v can be comparable to fa2, the moments corresponding to the former may be much smaller than those corresponding to the latter.

It should be noted that, for all the computed cases using

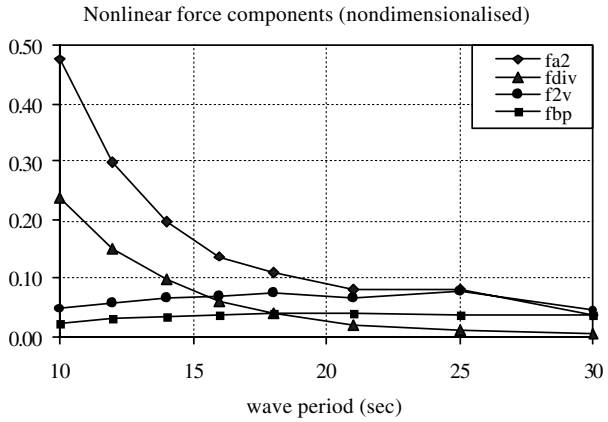

Fig. 8. Non-linear force components via wave period ($H = 9$ m).

monochromatic waves, the non-linear components oscillate mainly at half the wave period, due to their second-order dominated behaviour, and are very small compared to the total forces.

As a consequence, these non-linear forces have a very small effect at and around the usual wave period range of from 4 to 20 s. However, there are also components of non-linear forces that arise at frequencies given by the difference in frequency components in the incident wave spectrum. Effects of these non-linear forces at difference frequencies are significant because they can excite responses in spar surge and pitch motions which tend to have relatively long natural periods compared to predominant wave periods. This surge and pitch response at resonance, when excited by difference frequency wave components, is the most critical design case for spar moorings. Also the resonant response and consequential mooring line loads are limited only by damping — making this a particularly important parameter requiring accurate estimation in this design case.

The non-linear forces at such difference frequencies are examined next by considering a bichromatic incident wave.

4.4. Spar response to bichromatic waves

Here, the spar is excited by a sum of two monochromatic

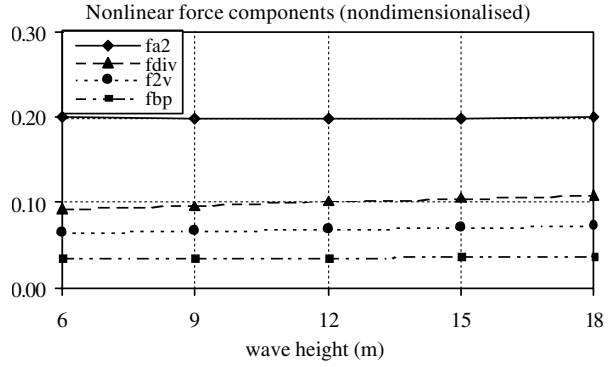

Fig. 9. Non-linear force components via wave height (wave period 14 s).

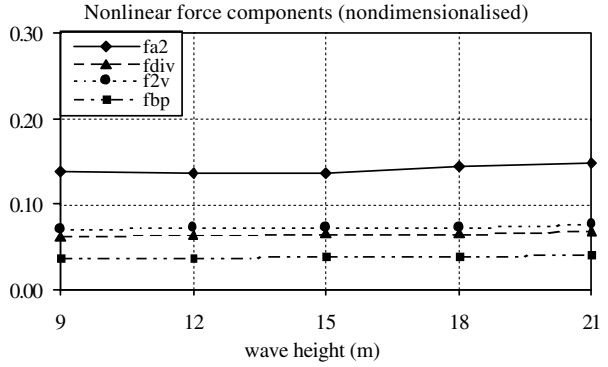

Fig. 10. Non-linear force components via wave height (wave period 16 s).

ocean waves with heights and periods expressed by (H_1, H_2) and (T_1, T_2), respectively. In the first case, the wave parameters are taken as $H_1 = H_2 = 12$ m, $T_1 = 14.00$ s and $T_2 = 13.43$ s. The period corresponding to the difference frequency of the two waves is about 330 s, which is close to the natural period of surge motion with the catenary moorings providing the necessary system stiffness. In order to investigate the non-linear effects of the resultant wave forces, Fourier analysis on the time history of the surge motion is carried out to obtain the non-linear slow motion (corresponding to the difference frequency wave). The result is presented in Fig. 11, where 'without f2v' denotes that the surge force and pitching moment with the centrifugal term are not included. A similar meaning is used for the 'without fdiv and f2v' labels. It can be seen from this figure that when the axial divergent and the centrifugal forces are all included, the slow surge motion is much larger than the motion without them. When the centrifugal force is not included, the difference is also visible but is not as marked. Similar results for the second case are presented in Fig. 12, in which $H_1 = H_2 = 12$ m, $T_1 = 16.17$ s and $T_1 = 17$ s; and the corresponding period of the different frequency is about 331 s. Again, when the axial divergent and the centrifugal forces are not included, the slow surge is much smaller than when the spar is excited by the force calculated with the full formulation. In this case, however, the influence of the centrifugal force on the surge motion is more evident. These two figures demonstrate that the influence of fidv and f2v on the responses may be important in many cases when the period corresponding to the difference frequency of incident waves is close to a natural period of the spar. The influence of fbp on the motions corresponding to the above two cases has also been investigated but its effect is not as large as that of fidv and f2v. This may be due to the fact that the amplitude of fbp in these cases is much smaller than those of fdiv and f2v. In addition, whether with or without fdiv and f2v, pitch motions (not presented here for brevity) differ very little from each other in these cases. This is primarily because the period of the non-linear forces is very different from that of the pitch motion.

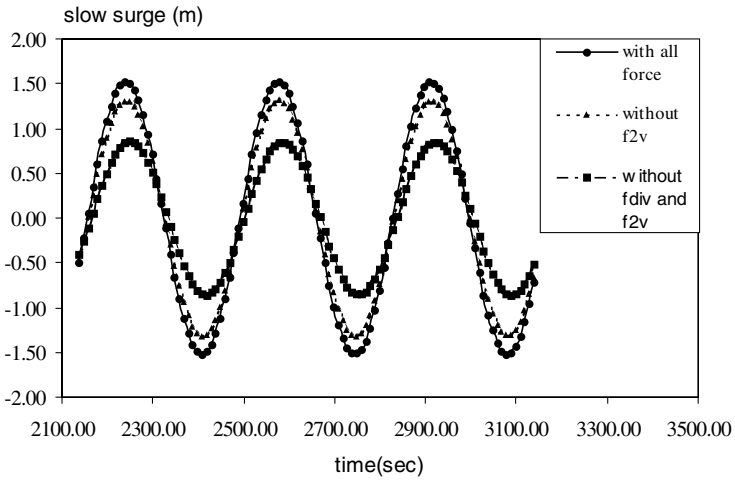

Fig. 11. Low Frequency surge at the centre of gravity due to a bichromatic wave ($H_1 = H_2 = 12$ m, $T_1 = 14$ s and $T_2 = 13.43$ s).

5. Conclusions

This paper has presented a formulation of the non-linear forces acting on spar platforms that includes the effects of some significant components that have been neglected in the past. The formulation calculates ocean wave forces on a spar based on Rainey [9,10] and combines these with a drag force calculation used in the Morison equation. These forces and the fully non-linear equations of motion have been solved using a fifth order Range–Kutta technique with adaptive step size control.

Once this full formulation was set up, it has been used to investigate the components of various non-linear forces on the spar. Particular attention has been paid to three force components — the so-called centrifugal force, the point force at the spar lower end and an axial-divergence force. The first two of these forces have not been included in computation on spar buoys reported in the literature. The last of these forces has been included although it has then been shown to be small for the wave conditions used and then neglected thereafter.

The work in this paper demonstrates that effects of the centrifugal and axial-divergence force components may be significant compared to those of the non-linear force due to wave acceleration. It is also shown that the magnitudes of these two forces components are strongly dependent on wave conditions and may be small in some circumstances but cannot be neglected in general. This point has a particular significance for the non-linear difference frequency forces which have a disproportionate effect on spar horizontal motions and mooring loads because they invariably are in a long period range capable of exciting mooring system resonance.

There is no significant difficulty or computational penalty in including these three force components — the centrifugal force, the point force at the lower end and the axial divergence force. It is recommended that they are included as part of the formulation for wave loads on all spar buoys.

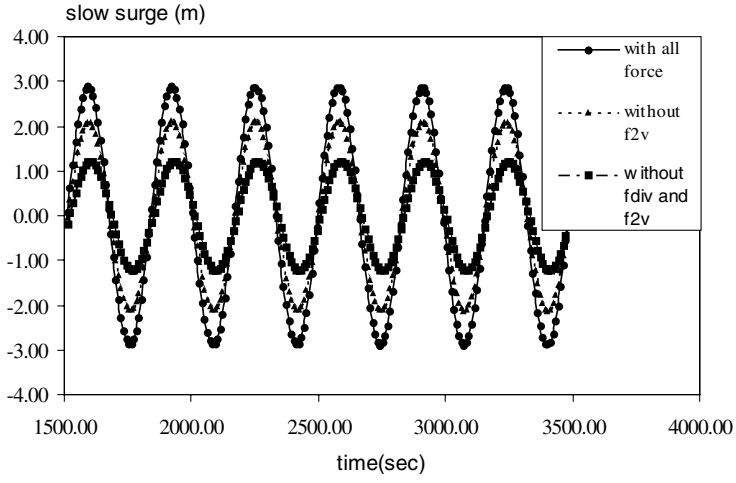

Fig. 12. Low frequency surge at the centre of gravity due to a bichromatic wave ($T_1 = 16$ s and $T_2 = 17.2$ s).

References

[1] Vardeman RD, Richardson S, McCandless CR. Neptune Project: Overview and Project management. OTC 8381, Offshore Technology Conference, Houston, TX, USA. Vol. 2, 1997. p. 227–35.

[2] Fisher FH, Spiess FN. Flip-floating instrument platform. J Acoust Soc Am 1963;35(10):1633–44.

[3] Halkyard JE. Status of Spar platform for deep water production system. ISOPE'96, Los Angeles, CA, USA. Vol. 1, 1996. p. 262–72.

[4] Glanville RS, Halkyard JE, Davies RL, Steen A, Frimm F. Neptune Project: Spar history and design considerations. OTC 8382, Offshore Technology Conference, Houston, TX, USA. Vol. 2, 1997. p. 237–51.

[5] Weggel DC, Roesset JM. Second-order dynamic response of s large spar platform: numerical predictions versus experimental results. OMAE'96, Florence, Italy. Vol. 1, Part A, 1996. p. 489–96.

[6] Carpenter EB, Leonard JW, Yim SCS. Experimental and numerical investigations of tethered spar and sphere buoys in irregular waves. Ocean Engng 1995;22(8):765–84.

[7] Ran Z, Kim MH, Zheng W. Coupled dynamic analysis of a moored spar in random waves and currents (time-domain vs. Frequency-domain analysis). OMAE'98, Lisbon, Portugal. Vol. 1, 1998.

[8] Chitrapu AS, Saha S, Salpekar VY. Time-domain simulation of spar platform response in random waves and current. OMAE'98, Lisbon, Portugal. Vol. 1, 1998.

[9] Rainey RCT. New equation for calculating wave loads on offshore structures. J Fluid Mech 1989;204:295–324.

[10] Rainey RCT. Slender-body expressions for the wave load on offshore structures. Proc R Soc London Ser A — Math Phys Sci 1995;450(1939):391–416.

[11] Mekha BB, Weggel DC, Johnson CP, Roesset JM. Effects of second order diffraction forces on the global response of spars. ISOPE'96, Los Angeles, CA, USA. Vol. 1, 1996. p. 273–80.

[12] Manners W, Rainey RCT. Hydrodynamic-forces on fixed submerged cylinders. Proc R Soc London Ser A — Math Phys Engng Sci 1992;436(1896):13–32.

[13] Kim MH, Chen W. Slender-body approximation for slowly-varying wave loads in multi-directional waves. Appl Ocean Res 1994;16:141–63.

[14] Ma QW. Numerical simulation of nonlinear interaction between structures and steep waves. PhD thesis. Department of Mechanical Engineering, University College London, 1998.

[15] Pauling JR, Webster WC. A consistent, large-amplitude analysis of the coupled response of TLP and Tendon system. OMAE'86, Tokyo, Japan. Vol. 3, 1986. p. 126–33.

[16] Shampine LF. Numerical solution of ordinary differential equations. Chapman and Hall Mathematics, 1994.